

randomly assigned to N₂-fixing and non-fixing treatments. Either N₂:O₂ or Ar:O₂ was delivered through perforated plastic tubing 1 cm above the base, at 100 ml min⁻¹. Three months after planting, nodules were removed from roots. Roots were cut, vortexed, and sonicated in a FS20 'watch-bath' type sonicator in 0.01% Tween 20. The extractant was diluted 10⁶-fold and spread on MAG antibiotic-containing plates. Intact nodules were removed from roots, counted, weighed and crushed in a tissue homogenizer, diluted and plated. Sand from each box was homogenized for 30 min in a sterile flask containing sterile 0.01% Tween 20, on a flask rotator. A liquid subsample was removed from the sand mixture 3 cm below the water line, diluted by 10⁴ and plated. Colonies grew for 10 d at 32 °C and colony-forming units (c.f.u., mean of eight plates) were recorded.

Split-root experiment

Seeds of *G. max* semidwarf variety 'S0066' were sterilized, germinated, and inoculated with approximately 10⁷ cells per seedling. Twelve plants, each with two similar root halves (resulting from regrowth after root-tip removal), were transplanted to hydroponic chambers, with similar nodule numbers on each half of a chamber divided by a silicone gel seal. Chamber halves were randomized into two treatments, either N₂:O₂ or Ar:O₂ (80:20, v/v) at 130 ml min⁻¹, 5 d after transplanting. H₂ production was measured to confirm disruption of N₂ fixation²⁹ by Ar:O₂. Five weeks after transplanting, roots, nodules and rhizobia in nutrient solution were processed as described above for the 12 replicates, each a paired comparison. For survival assays, nodule homogenate was diluted and added at an estimated 10⁵ rhizobia per g sterile sand. Twenty weeks later, rhizobial populations were determined by plate counts.

Single-nodule experiment

Six independent replicate experiments used *G. max* 'S0066' grown in plastic growth pouches and inoculated as above. Fifteen days later, two nodules of equal size were selected per plant. Fixing and non-fixing treatments were randomized. Chambers of 2 cm diameter were positioned around intact nodules, with 250 ml min⁻¹ of humidified N₂:O₂ or Ar:O₂ flowing through each chamber. Fractional oxygenation of leghaemoglobin under air, nodule O₂ permeability, and O₂-saturated respiration rate were measured daily as previously described^{23,30}. Briefly, nodules were exposed successively to 20, 0, 70 and 0% O₂ while fractional oxygenation of the nodule protein leghaemoglobin was measured by non-invasive spectrophotometry. O₂ permeability was calculated from the rate of increase in oxygenation after switching to 70% O₂, after correcting for respiration, which was calculated from the rate of oxygenation decrease as interior O₂ fell from O₂-saturated to O₂-limited concentrations after switching to 0% O₂. After 10 d, nodules were weighed, crushed, and assayed for c.f.u. per nodule and per g of nodule. Analyses of variance and Tukey's studentized range test for whole-root, and paired *t*-tests for split-root and single nodule experiments were conducted using SAS software (SAS Institute).

Received 9 May; accepted 18 July 2003; doi:10.1038/nature01931.

1. Herre, E. A., Knowlton, N., Mueller, U. G. & Rehner, S. A. The evolution of mutualisms: exploring the paths between conflict and cooperation. *Trends Ecol. Evol.* **14**, 49–53 (1999).
2. Frank, S. A. *Foundations of Social Evolution* (Princeton Univ. Press, Princeton, 1998).
3. Yu, D. W. Parasites of mutualisms. *Biol. J. Linn. Soc.* **72**, 529–546 (2001).
4. Axelrod, R. & Hamilton, W. D. The evolution of cooperation. *Science* **211**, 1390–1396 (1981).
5. Denison, R. F. Legume sanctions and the evolution of symbiotic cooperation by rhizobia. *Am. Nat.* **156**, 567–576 (2000).
6. West, S. A., Kiers, E. T., Simms, E. L. & Denison, R. F. Sanctions and mutualism stability: why do rhizobia fix nitrogen? *Proc. R. Soc. Lond. B* **269**, 685–694 (2002).
7. Crespi, B. J. The evolution of social behavior in microorganisms. *Trends Ecol. Evol.* **16**, 178–183 (2001).
8. West, S. A., Kiers, E. T., Pen, I. & Denison, R. F. Sanctions and mutualism stability: when should less beneficial mutualists be tolerated? *J. Evol. Biol.* **15**, 830–837 (2002).
9. Pellmyr, O. & Huth, C. J. Evolutionary stability of mutualism between yuccas and yucca moths. *Nature* **372**, 257–260 (1994).
10. Frank, S. A. Mutual policing and repression of competition in the evolution of cooperative groups. *Nature* **377**, 520–522 (1995).
11. Ratnieks, F. L. W., Monnin, T. & Foster, K. R. Inclusive fitness theory: novel predictions and tests in social Hymenoptera. *Ann. Zool. Fennici* **38**, 201–214 (2001).
12. Burdon, J. J., Gibson, A. H., Searle, S. D., Woods, M. J. & Brockwell, J. Variation in the effectiveness of symbiotic associations between native rhizobia and temperate Australian *Acacia*: within-species interactions. *J. Appl. Ecol.* **36**, 398–408 (1999).
13. Singleton, P. W. & Stockinger, K. R. Compensation against ineffective nodulation in soybean. *Crop Sci.* **23**, 69–72 (1983).
14. Ferriere, R., Bronstein, J. L., Rinaldi, S., Law, R. & Gauduchon, M. Cheating and the evolutionary stability of mutualisms. *Proc. R. Soc. Lond. B* **269**, 773–780 (2001).
15. Amarger, N. Competition for nodule formation between effective and ineffective strains of *Rhizobium meliotti*. *Soil Biol. Biochem.* **13**, 475–480 (1981).
16. Hahn, M. & Studer, D. Competitiveness of a *nif⁻* *Bradyrhizobium japonicum* mutant against the wild-type strain. *FEMS Microbiol. Lett.* **33**, 143–148 (1986).
17. Rasche, M. E. & Arp, D. J. Hydrogen inhibition of nitrogen reduction by soybean in isolated soybean nodule bacteroids. *Plant Physiol.* **91**, 663–668 (1989).
18. Singleton, P. W. & van Kessel, C. Effect of localized nitrogen availability to soybean half-root systems on photosynthate partitioning to roots and nodules. *Plant Physiol.* **83**, 552–556 (1987).
19. Udvardi, M. K. & Kahn, M. L. Evolution of the (*Brady*)*Rhizobium*-legume symbiosis: why do bacteroids fix nitrogen? *Symbiosis* **14**, 87–101 (1993).
20. King, B. J. & Layzell, D. B. Effect of increases in oxygen concentration during the argon-induced decline in nitrogenase activity in root nodules of soybean. *Plant Physiol.* **96**, 376–381 (1991).
21. Sheehy, J. E., Minchin, F. R. & Witty, J. F. Biological control of the resistance to oxygen flux in nodules. *Ann. Bot.* **52**, 565–571 (1983).

22. Hartwig, U., Boller, B. & Nösberger, J. Oxygen supply limits nitrogenase activity of clover nodules after defoliation. *Ann. Bot.* **59**, 285–291 (1987).
23. Denison, R. F. & Harter, B. L. Nitrate effects on nodule oxygen permeability and leghemoglobin. Nodule oximetry and computer modeling. *Plant Physiol.* **107**, 1355–1364 (1995).
24. Layzell, D. B., Rainbird, R. M., Atkins, C. A. & Pate, J. S. Economy of photosynthetic use in nitrogen-fixing legume nodules. *Plant Physiol.* **64**, 888–891 (1979).
25. Sen, D. & Weaver, R. W. Nitrogen fixing activity of rhizobial strain 32H1 in peanut and cowpea nodules. *Plant Sci. Lett.* **18**, 315–318 (1980).
26. Ludwig, E. M. *et al.* Amino-acid cycling drives nitrogen fixation in the legume–*Rhizobium* symbiosis. *Nature* **422**, 722–726 (2003).
27. Kijne, J. W. The fine structure of pea root nodules. 2. Senescence and disintegration of the bacteroid tissue. *Physiol. Plant Pathol.* **7**, 17–21 (1975).
28. Sprent, J. I. & Raven, J. A. Evolution of nitrogen-fixing symbioses. *Proc. R. Soc. Edinb. B* **85**, 215–237 (1985).
29. Layzell, D. B., Hunt, S., King, B. J., Walsh, K. B. & Weagle, G. E. in *Applications of Continuous and Steady-State Methods to Root Biology* (eds Torrey, J. G. & Winship, L. J.) 1–28 (Kluwer Academic, Dordrecht, 1989).
30. Denison, R. F. & Layzell, D. B. Measurement of legume nodule respiration and O₂ permeability by noninvasive spectrophotometry of leghemoglobin. *Plant Physiol.* **96**, 137–143 (1991).

Acknowledgements We thank R. Grosberg, S. Nee, A. Griffin, D. Shuker and M. Stanton for comments, P. Graham, D. Phillips and M. King for advice on methods, R. Nelson and D. Smith for soybean cultivars 'T243' and 'S0066', and P. van Berkum for *B. japonicum* 110ARS. This work was supported by the NSF (grant to R.E.D. and graduate fellowship to E.T.K.), the California Agricultural Experiment Station, the Land Institute, the Royal Society, the BBSRC and the NERC.

Competing interests statement The authors declare that they have no competing financial interests.

Correspondence and requests for materials should be addressed to R.E.D. (rfdenison@ucdavis.edu).

.....
Functional genetic analysis of mouse chromosome 11

Benjamin T. Kile^{1*}, Kathryn E. Hentges^{1*}, Amander T. Clark^{1*}, Hisashi Nakamura¹, Andrew P. Salinger¹, Bin Liu¹, Neil Box¹, David W. Stockton¹, Randy L. Johnson², Richard R. Behringer³, Allan Bradley^{1†} & Monica J. Justice¹

¹Department of Molecular and Human Genetics, Baylor College of Medicine, One Baylor Plaza, Houston, Texas 77030, USA
²Department of Biochemistry and Molecular Biology, and ³Department of Molecular Genetics, University of Texas M.D. Anderson Cancer Center, Houston, Texas 77030, USA

*These authors contributed equally to this work
[†] Present address: The Wellcome Trust Sanger Institute, Hinxton, Cambridge, CB10 1SA, UK

.....
Now that the mouse and human genome sequences are complete, biologists need systematic approaches to determine the function of each gene^{1,2}. A powerful way to discover gene function is to determine the consequence of mutations in living organisms. Large-scale production of mouse mutations with the point mutagen N-ethyl-N-nitrosourea (ENU) is a key strategy for analysing the human genome because mouse mutants will reveal functions unique to mammals, and many may model human diseases³. To examine genes conserved between human and mouse, we performed a recessive ENU mutagenesis screen that uses a balancer chromosome, inversion chromosome 11 (refs 4, 5). Initially identified in the fruitfly, balancer chromosomes are valuable genetic tools that allow the easy isolation of mutations on selected chromosomes⁶. Here we show the isolation of 230 new recessive mouse mutations, 88 of which are on chromosome 11. This genetic strategy efficiently generates and maps mutations on a single chromosome, even as mutations throughout the genome are discovered. The mutations reveal new defects in haematopoiesis, craniofacial and cardiovascular development, and fertility.

Table 1 Eighty-eight new mutants on mouse chromosome 11

Category	Number new*	Locus name	Phenotype	Number known†	
Lethal	6	<i>I11Jus1,-2,-3,-4,-7,-12</i>	Prenatal death post implantation, before E9.5	5	
	12	<i>I11Jus5,-6,-8,-9,-11,-14,-17-20,-27,-39</i>	Prenatal death E9.5–12.5	6	
	2	<i>I11Jus15,-29</i>	Prenatal death after E12.5	3	
	10	<i>I11Jus24,-30,-32,-34-38,-42,-46</i>	Prenatal death, stage not determined		
	23	<i>I11Jus10,-13,-16,-21-23,-25,-26,-31,-33,-40,-41,-43,-44,-47,-48,-51-57</i>	Postnatal death	8	
	2	<i>I11Jus28,-45</i>	Time of death unknown		
	10	<i>nur1,-2</i>	Nervousness, tremors	6	
Neurological		<i>nur3,-6</i>	Small, hyperactive		
		<i>nur4,-5</i>	Tremors		
		<i>nur7</i>	Small, lethargic, tremors in adults		
		<i>nur8</i>	Epilepsy, craniofacial, eye		
		<i>nur9</i>	Weaving head/hearing loss		
		<i>nur10</i>	Small, splayed gait		
	Skeletal: craniofacial	5	<i>crf2,-3,-5,-8,-12</i>	Craniofacial abnormalities	1‡
	Skin/coat	2	<i>skc1,-2</i>	Coat texture	1§
	Growth/size	5	<i>gro1</i>	Small at P9 to adult	2
			<i>gro22</i>	Small, low cholesterol	
		<i>gro40</i>	Small, half size		
		<i>gro41</i>	Small, sickly		
		<i>gro42</i>	Small, two-thirds size		
Infertility		6	<i>inf2,-4-6,-8,-9</i>	Male infertility	1
	2	<i>inf3,-7</i>	Female infertility	0	
Haematopoietic	3	<i>hem1,-3</i>	Immature WBCs	2	
		<i>hem2</i>	Anaemia		

Locus names are derived from the underlined letters.

*The number of each phenotype isolated in this ENU screen. These mouse mutants are available to the scientific community on request at <http://www.mouse-genome.bcm.tmc.edu>.

†The number of previously reported spontaneous or targeted mutants that lie in the *Trp53-Wnt3* region²⁸. An additional six mutations had phenotypes detected by assays not performed in this screen to make a total of 45 mutations with phenotypes reported. Twenty-one targeted mutations in this region were reported as having no phenotype.

‡Four additional mutations with skeletal phenotypes were reported.

§One recessive coat colour mutation was reported.

Genetic strategies that can isolate mouse mutations in regions that are conserved between the mouse and human provide ways to infer the function of human genes. Human chromosome 17 genes that are conserved in the mouse are located on mouse chromosome 11. The inversion chromosome 11 (Inv(11)8Brd^{*Trp53-Wnt3*}; Fig. 1a)

balancer has properties that allow us to isolate mutations on chromosome 11 after a three-generation breeding scheme (Fig. 1b), even though mutations induced by ENU will occur throughout the genome of the treated male (genome-wide mutations recovered are summarized in Supplementary Table 1).

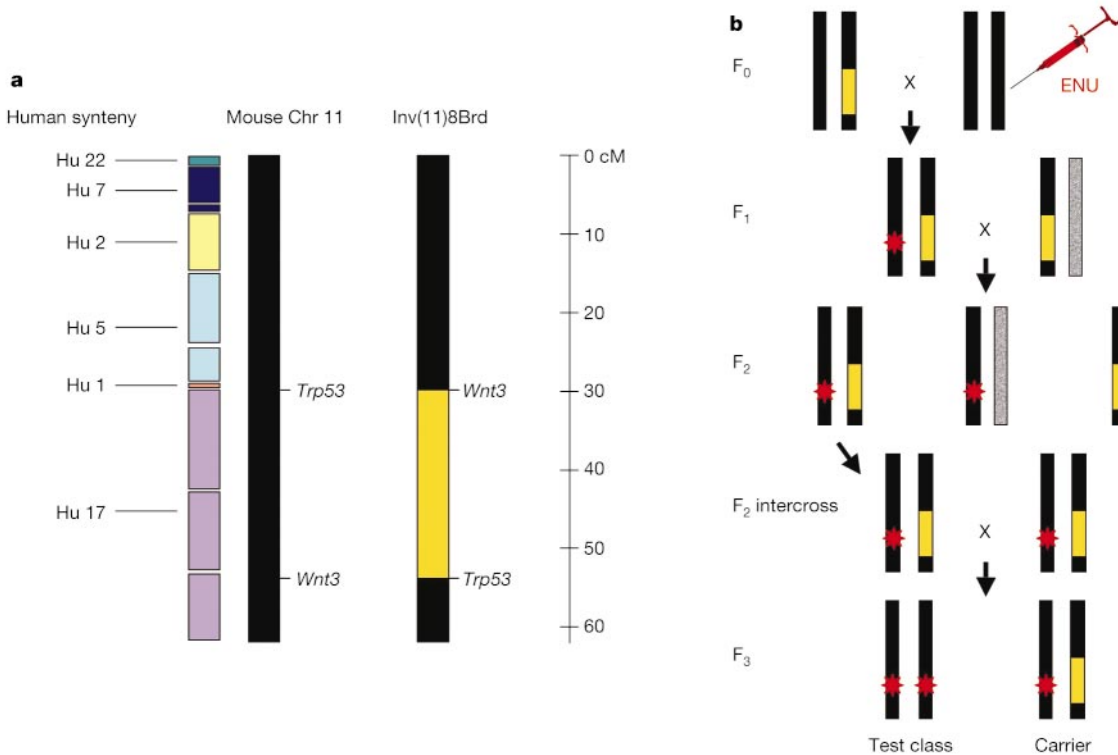


Figure 1 A balancer chromosome screen for the conserved region of mouse chromosome 11/human chromosome 17. **a**, The distal two-thirds of mouse chromosome 11 is conserved with human chromosome 17 (purple)¹. The Inv(11)8Brd^{*Trp53-Wnt3*} balancer contains a 24-cM inversion (34 Mb; yellow box) between *Trp53* and *Wnt3* on mouse chromosome 11. **b**, ENU-treated C57BL/6J males (black chromosomes) are mated to females carrying the balancer (yellow box; *K14-Agouti* produces yellow ears, tail and

ventrum) to generate first generation (F₁) animals that may carry a new mutation (red asterisk). F₁ animals are mated to mice carrying a balancer and *Rex* (dominant curly coat, grey chromosome), which marks the non-mutagenized chromosome. Informative F₂ animals identified by their yellowish colour and lack of curly coat are mated to look for new mutations (two asterisks; test class) in the F₃ offspring. Mice homozygous for the inversion are *Wnt3*-deficient and die by E10.5 (not shown).

For example, *Inv(11)8Brd^{Trp53-Wnt3}* contains a 24-cM inversion on mouse chromosome 11 between the *Trp53* and *Wnt3* genes that suppresses the recovery of recombination products over nearly half of the chromosome. Thus, mutations induced in a wild-type chromosome will remain fixed when maintained *in trans* to the balancer in heterozygous animals. The inversion has a dominant *Agouti* coat colour marker, which allows animals that carry it to be easily identified. Therefore, heterozygotes and mutant homozygotes can be easily distinguished by their coat colour.

In contrast to previous mouse recessive ENU screens that focused on a single stage of embryogenesis⁷⁻⁹, our genetic screen using the *Inv(11)8Brd^{Trp53-Wnt3}* balancer is designed to isolate all lethal mutations from fertilization to adulthood, because the simple absence of test class animals (those lacking the *Agouti* transgene) identifies a lethal mutation. Fifty-five of the mouse chromosome 11 mutants are lethal when homozygous (Table 1). Thirty pedigrees carry mutations that cause prenatal death, whereas 23 pedigrees carry mutations that cause postnatal death (Supplementary Table 2). Many of the postnatal lethal mutations exhibit visible pheno-

types such as small size, developmental delay, craniofacial or neurological abnormalities (Supplementary Fig. 1 and movie). Lethal mutations are the most common phenotypic class isolated in model organisms such as *Caenorhabditis elegans* and *Drosophila*^{10,11}. Approximately 60% of the mouse chromosome 11 mutations identified in this screen are lethal in homozygotes, and nearly one-half of the spontaneous or targeted mutations in the balancer interval are lethal (Table 1). Two mutagenesis screens that would isolate mutations in a defined genomic region have been carried out previously in the mouse, and each of these screens yielded primarily lethal mutations^{12,13}. Together, these data suggest that many mouse mutations are detrimental to the survival of the animal. One end of *Inv(11)8Brd^{Trp53-Wnt3}* disrupts *Wnt3*, causing embryonic lethality in mice homozygous for the balancer. Combined with the property of recombination suppression, this allows lethal mutations to be easily maintained *in trans* through heterozygous crosses, without requiring molecular markers for stock maintenance.

Further analysis of the cause of death of the lethal mutations revealed a broad range of distinctive phenotypes at every stage of development (Fig. 2; see also Supplementary Fig. 2). Some chromosome 11 mutants exhibited abnormal somite morphology or neural tube defects (*l11Jus5,-8,-15,-39*), which are often observed in human birth defects. Others, such as *l11Jus3*, had abnormal visceral endoderm cells and failed to gastrulate (Fig. 2a, b). However, most of the phenotypes are the result of defects in organs and tissues such as heart, blood vessels, placenta, or haematopoietic cells. For example, *l11Jus27* mutants have distended tubular hearts (Fig. 2c, d). No mutations that cause such a defect map to mouse chromosome 11, implying that *l11Jus27* identifies a new gene required for cardiac development¹⁴. *l11Jus15* homozygotes develop a severe oedema, suggesting a circulatory defect (Fig. 2e, f). *l11Jus51* homozygotes exhibit a severe anaemia at birth (Fig. 2g). Just as *Drosophila* lethal mutants have been valuable for dissecting the molecular basis for embryonic patterning¹⁵, these mouse mutations will be valuable for identifying new genes that function in cardiovascular and haematopoietic development.

In addition to the lethal mutants, an additional 24 pedigrees produced phenotypes segregating on mouse chromosome 11 that affect coat, growth/size, skeletal morphology, blood cell abnormalities, or neurological presentation (Table 1; see also Supplementary Table 3). Nine of the mutations isolated on chromosome 11 exhibit severe craniofacial defects, sometimes accompanied by other abnormalities such as seizures and growth defects (craniofacial *crf2,-6,-5,-8,-12*; neurological *nur8, l11Jus52,-53* and *-54*). With the exception of a craniofacial defect observed in a *Hoxb2* knockout mouse¹⁶, no mouse craniofacial defects have been reported previously on this chromosome. Several human diseases with craniofacial defects map to the region of conserved synteny on human chromosome 17, including Meckel syndrome (OMIM number 24900), lethal microcephaly (OMIM number 607196), mulibrey nanism (OMIM number 253250) and Alexander disease (OMIM number 203450), suggesting that our mutants may be new models of human disease.

A screen for infertility on a subset of 184 pedigrees identified eight pedigrees exhibiting infertile or sub-fertile phenotypes mapping to chromosome 11. Six mutations resulted in male sterility with reduced sperm counts (infertility *inf2,-4,-5,-6,-8,-9*). Histopathology revealed blocks in spermatogenesis in *inf4, inf8* and *inf9* males that occurred between round spermatid formation (*inf9*) and late differentiating spermatids (*inf4*; Supplementary Fig. 3). Cysts in multiple organs, including kidney, testis and liver, led to a male sub-fertile phenotype in one mutant, *inf6*, but was not a primary male infertility defect.

The ENU mutation rate in mouse spermatogonial stem cells is one new mutation per locus in every 700 gametes or mutagenized genomes screened¹⁷. Therefore, by screening 735 pedigrees, we have

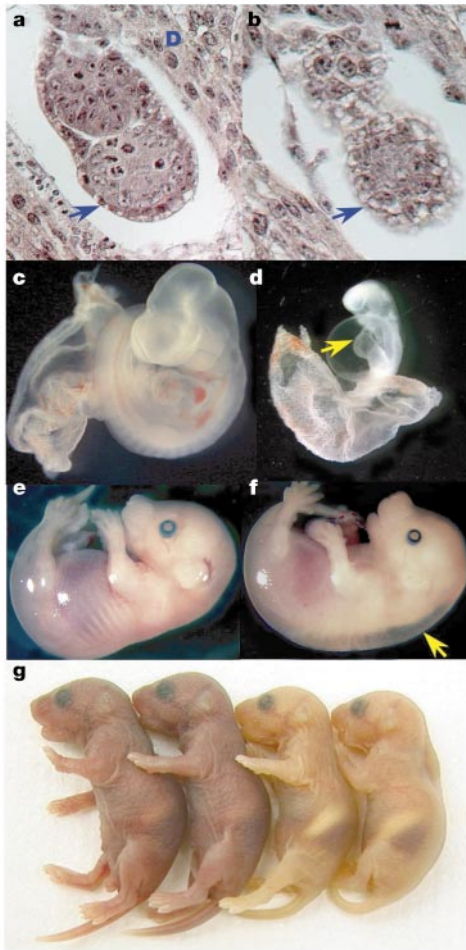


Figure 2 Lethal mutants affect gastrulation and cardiovascular development. **a**, Wild-type embryos at E5.5 develop within the maternal decidua (D), and have well-developed cuboidal epithelium that defines the visceral endoderm (blue arrow). **b**, *l11Jus3* homozygotes have abnormal visceral endoderm and arrest before gastrulation (blue arrow). **c**, Wild-type embryos at E10.0 have well-developed hearts. **d**, *l11Jus27* homozygotes have distended tubular hearts (yellow arrow). **e**, Wild-type embryo at E16.5. **f**, *l11Jus15* homozygotes develop a severe oedema (arrow). **g**, *l11Jus51* homozygotes (right) are pale at birth compared with wild-type littermates (left).

sampled one genome equivalent for this region of mouse chromosome 11. In such a sample, some genes may not have been mutated in any pedigree, whereas others may have been mutated in multiple pedigrees. Consistent with this prediction, obvious visible mutant phenotypes of genes on mouse chromosome 11, such as headless embryos (*Lhx1*)¹⁸, circling behaviour (*Myo15*)¹⁹ and hairless mice (*Foxn1*)²⁰ have not been isolated. In addition, we performed pairwise complementation crosses on mutants in similar phenotypic classes (Supplementary Tables 4 and 5). Of 24 lethal mutations completed, only two (*I11Jus1* and *I11Jus4*) fail to complement each other. These data demonstrate that the great majority of these mutations are in independent genes. It is likely that most of the mutations are in genes not previously mutated or are new alleles of known genes, because most of the developmental and neurological phenotypes do not mimic the phenotypes described in the 45

targeted or spontaneous mutations (Table 1).

Chemical mutagenesis can cause multiple mutations in a single pedigree. The likelihood that linked lethal mutations are being recovered provides an estimate of how commonly linked mutations occur. If we assume a Poisson distribution, a total of 7.4% of chromosome 11 transmissions will carry one lethal mutation, which is not statistically different from the number observed (7.5%; $\chi^2 = 0.008$; $P > 0.90$). The likelihood of a chromosome containing two lethal mutations at the dose of $3 \times 100 \text{ mg kg}^{-1}$ in the C57BL/6J strain is only 3 in 1,000. This is very different from screens in *Drosophila* where over 80% of the chromosomes were predicted to contain one or more lethal mutations when administered a dose of 25 mM ethylmethanesulphonate²¹. The difference can be explained because one whole *Drosophila* chromosome covered by a balancer, such as chromosome 2, contains nearly

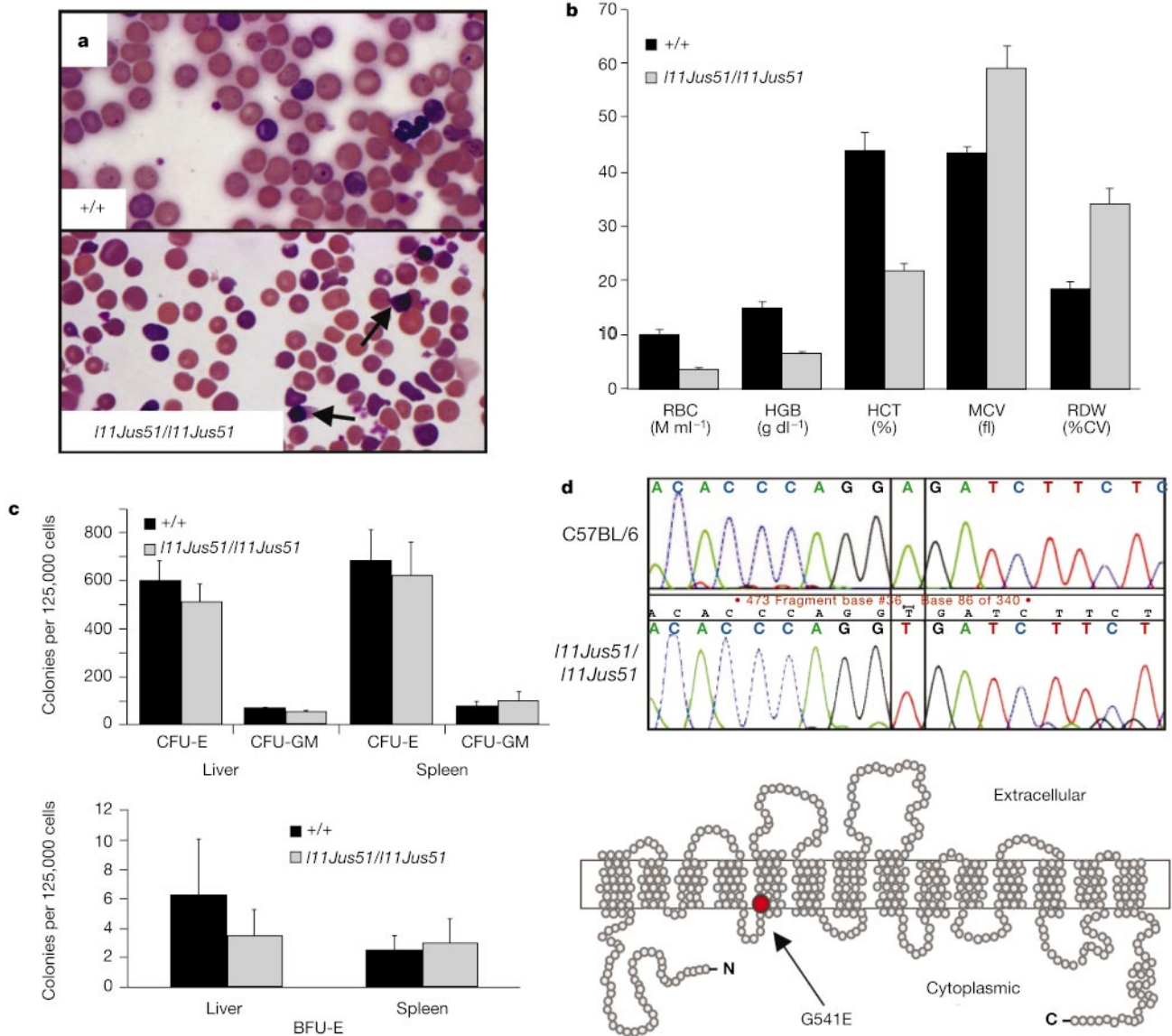


Figure 3 A new *Slc4a1* missense mutation. **a**, Peripheral blood smears from 2-day-old *I11Jus51* homozygotes have nucleated erythroid cells (arrows). **b**, CBC analysis of 8-week-old *I11Jus51* homozygotes shows decreases in erythrocyte numbers (RBC), haemoglobin (HGB) and haematocrit (HCT), with increased mean corpuscular volume (MCV) and red blood cell distribution width (RDW). %CV, % corpuscular volume.

c, Methylcellulose cultures of fetal liver and spleen reveal no differences in progenitor cell numbers and kinetics. CFU-E, colony-forming unit erythroid; CFU-GM, colony forming unit granulocyte/macrophage; BFU-E, burst-forming unit erythroid. **d**, Sequencing *Slc4a1* in *I11Jus51* homozygotes reveals an A-to-T transversion at coding nucleotide 1622, resulting in a glutamic acid to valine change.

35% of the fly genome, whereas our screen targets approximately 2% of the mouse genome. For our screen, the Poisson calculation suggests that the probability of a linked mutation interfering with the phenotype of another is very low.

One benefit of the balancer chromosome is that mutations within the inversion interval are mapped on their isolation, without further crosses, allowing for immediate analysis of candidate genes. For example, *111Jus51* maps within the balancer interval and 80–90% of homozygous animals die within one week of birth with a severe anaemia (Fig. 2g). Red blood cell morphology is abnormal, and large numbers of nucleated erythroid cells are present in the circulation (Fig. 3a). Rare adult survivors have a macrocytic anaemia, with decreased haemoglobin, haematocrits and red blood cell numbers (Fig. 3b). *In vitro* haematopoietic colony assays of fetal liver and spleen reveal that erythroid progenitor cells are present in normal numbers and possess normal proliferative potential, suggesting that the anaemia is due to abnormal destruction or loss of red blood cells, and not to a defect in production (Fig. 3c). An analysis of the databases shows several genes involved in erythrocyte maturation or maintenance in the balancer interval; most notable is solute carrier protein 4a1 (*Slc4a1*; also known as band 3 or anion exchange protein 1). Two targeted mutations eliminating this protein result in a severe microcytic anaemia with altered red blood cell membrane fragility^{22,23}. We investigated the possibility that *111Jus51* carried a mutation in *Slc4a1* by performing a cross with the loss of function allele²², which revealed that *111Jus51* fails to complement the mutation. Subsequent sequencing revealed a missense mutation in the codon for amino acid 541, a residue conserved between mouse and human, changing a glutamic acid to a valine within the fifth transmembrane domain (Fig. 3d). Notably, mutations in *SLC4A1* are associated with hereditary spherocytosis and resistance to malarial infection in humans²⁴. Many of the missense disease mutations in human *SLC4A1* cause an autosomal dominant form of the disease that results in renal tubular acidosis^{25,26}. *111Jus51* is the first mouse missense mutation in *Slc4a1*, and causes a macrocytic anaemia rather than a microcytic anaemia as in the deletion alleles, suggesting that it will be useful for dissecting the biochemical basis of the loss of protein function without its complete absence. In addition, preliminary histopathology reveals kidney abnormalities; therefore, *111Jus51* may prove valuable as a mouse model for renal tubular acidosis.

New mouse mutations are the key to functional genomic studies that will unravel mammalian systems biology. Genome sequencing shows that the mammalian genome contains fewer genes than previously predicted¹. However, transcriptome and proteome analysis suggests that higher organism complexity is produced not by an increase in the absolute number of genes but by changes in temporal and spatial transcript expression, as well as alternative transcript and protein isoform production²⁷. Because ENU mutagenesis is phenotype-driven, it is a powerful way to discover gene function because no prior assumptions are made regarding a particular transcript or protein product. Although the *Trp53–Wnt3* interval of mouse chromosome 11 is predicted to contain over 700 genes and already has a large number of knockout mutations²⁸, we have tripled the number of mutants in this region with a one-genome coverage screen. The recovery of 142 mutations on other mouse chromosomes demonstrates that the balancer mutagenesis strategy has multiple benefits for the efficient functional annotation of the mammalian genome. □

Methods

Mouse strains

Inv(11)8Brd^{1Trp53–Wnt3} was engineered in 129/SvEv embryonic stem cells, and is maintained by subsequent backcrosses onto the inbred strains C57BL/6J (11 generations), 129S6/SvEvTac (8 generations) and C3HeB/FeJ (6 generations). Most pedigrees screened for mutations used 129.Inv(11)8Brd. The *Rex* mutation was acquired from The Jackson

Laboratory as the RSV/Le stock, and was subsequently backcrossed to make it congenic ($N > 10$) on the same three strains.

Mutagenesis and screening

C57BL/6J males (Jackson Laboratory) were injected intraperitoneally at the age of 8–10 weeks with 100 mg ENU per kg body weight weekly for three weeks³. Forty-seven fertile treated males were mated as in Fig. 1b. Of 905 F₁ animals, 735 produced enough litters at the third (F₃) generation to test that pedigree for phenotypes. A pedigree was bred as a potential new mutation if: (1) no test class animals were observed in a total of 24 carrier animals ($\chi^2 = 10.5$; $P < 0.01$); (2) all test class animals exhibited a similar phenotype; or (3) at least two or more animals of test or carrier class exhibited the same phenotype in a single pedigree. Additional phenotypes were found by letting the animals age to 3 months, performing complete blood counts (CBCs) with a differential analysis of white blood cells on 517 pedigrees²⁹, or testing for infertility in 184 pedigrees. Additional pedigrees were screened for biochemical, bone or soft tissue abnormalities (see Supplementary Information for phenotyping details).

Characterization of lethal mutants

If a pedigree produced no test class animals in a cohort of at least 24 carriers, the carrier class animals were used to generate a stock of mice. To eliminate any interfering phenotypes or accessory mutations in the pedigree, carrier animals were out crossed at least once to C3H.Inv(11)8Brd/*Re* animals, and then *Inv/m* animals were intercrossed to recover the original mutation. To determine the stage of death, timed matings were performed on carrier females by examining them each morning for a vaginal plug. Evidence of a plug was designated embryonic day (E)0.5, and females were killed for embryo examination at various stages. Mutant embryos were fixed in Bouin's fixative, embedded in paraffin, sectioned at 5 μ m, and stained with haematoxylin and eosin as previously described³⁰. Using PCR, embryos were genotyped for the presence of the human HPRT cassette present in the engineered inversion. DNA was prepared from embryonic tail or yolk sac samples and PCR was performed as a multiplex reaction with primers to the HPRT mini gene to detect the inversion chromosome and primers to mouse BAC clone RPC123–132B20 T7 end as a control for the presence of DNA. Conditions and primer sequences are available on request.

Sequencing

After PCR amplification, genomic DNA prepared from tails was sequenced directly using BigDye Terminators v3.0 (Applied Biosystems) according to the manufacturer's instructions. All *Slc4a1* exons and splice junctions were sequenced in their entirety in multiple homozygous *111Jus51* animals and the treated strain C57BL/6J; oligonucleotide primer sequences are available on request. No differences between *111Jus51* and C57BL/6J sequences were detected other than the A-to-T transversion at coding nucleotide 1622, which abolishes a *Bgl*III endonuclease restriction site.

Statistics and web display

Poisson distribution calculations were based on the observation of 55 lethal mutations in 735 pedigrees. Thus, $P(0) = e^{-m} = 0.925$, $m = 0.08$; $P(1) = 0.074$; $P(2) = 0.003$; $P(3) = 0.00008$. χ^2 tests are calculated with Yates' correction. See <http://www.mouse-genome.bcm.tmc.edu> (linked to a relational database) for phenotype information on the mutants generated from this mutagenesis screen. The interface to retrieve data from the SQL server was developed using Active Server Pages (ASP). Users can query mutant and map location, retrieve phenotype information and request mutants from this web page. An image management system, ImageView, allows public viewing of images. Movies can be viewed after registration on the web page.

Received 26 March; accepted 10 June 2003; doi:10.1038/nature01865.

1. Mouse Genome Sequencing Consortium. Initial sequencing and comparative analysis of the mouse genome. *Nature* **420**, 520–562 (2002).
2. International Human Genome Sequencing Consortium. Initial sequencing and analysis of the human genome. *Nature* **409**, 860–921 (2001).
3. Justice, M. J. in *Genetics and Transgenics: A Practical Approach* (eds Jackson, I. & Abbott, C.) 185–215 (Oxford Univ. Press, Oxford, 1999).
4. Zheng, B. *et al.* Engineering a balancer chromosome in the mouse. *Nature Genet.* **22**, 375–378 (1999).
5. Zheng, B., Mills, A. A. & Bradley, A. A system for rapid generation of coat color-tagged knockouts and defined chromosomal rearrangements in mice. *Nucleic Acids Res.* **27**, 2354–2360 (1999).
6. Muller, H. J. Genetic variability, twin hybrids, and constant hybrids, in a case of balanced lethal factors. *Genetics* **3**, 422–499 (1918).
7. Kasarskis, A., Manova, K. & Anderson, K. V. A phenotype-based screen for embryonic lethal mutations in the mouse. *Proc. Natl Acad. Sci. USA* **95**, 7485–7490 (1998).
8. Hentges, K., Thompson, K. & Peterson, A. The flat-top gene is required for the expansion and regionalization of the telencephalic primordium. *Development* **126**, 1601–1609 (1999).
9. Herron, B. J. *et al.* Efficient generation and mapping of recessive developmental mutations using ENU mutagenesis. *Nature Genet.* **30**, 185–189 (2002).
10. Kamath, R. S. *et al.* Systematic functional analysis of the *Caenorhabditis elegans* genome using RNAi. *Nature* **421**, 231–237 (2003).
11. Miklos, G. L. & Rubin, G. M. The role of the genome project in determining gene function: insights from model organisms. *Cell* **86**, 521–529 (1996).
12. Shedlovsky, A., King, T. R. & Dove, W. F. Saturation germ line mutagenesis of the murine *t* region including a lethal allele at the *quaking* locus. *Proc. Natl Acad. Sci. USA* **85**, 180–184 (1988).
13. Rinchik, E. M. & Carpenter, D. A. *N*-ethyl-*N*-nitrosourea mutagenesis of a 6- to 11-cM subregion of the *Fah-Hbb* interval of mouse chromosome 7: completed testing of 4,557 gametes and deletion mapping and complementation analysis of 31 mutations. *Genetics* **152**, 373–383 (1999).

14. Conway, S. J., Kruzynska-Frejtag, A., Kneer, P. L., Machnicki, M. & Koushik, S. V. What cardiovascular defect does my prenatal mouse mutant have, and why? *Genesis* **35**, 1–21 (2003).

15. Nusslein-Volhard, C., Frohnhof, H. G. & Lehmann, R. Determination of anteroposterior polarity in *Drosophila*. *Science* **238**, 1675–1681 (1987).

16. Barrow, J. R. & Capecchi, M. R. Targeted disruption of the *Hoxb-2* locus in mice interferes with expression of *Hoxb-1* and *Hoxb-4*. *Development* **122**, 3817–3828 (1996).

17. Hitotsumachi, S., Carpenter, D. A. & Russell, W. L. Dose-repetition increases the mutagenic effectiveness of *N*-ethyl-*N*-nitrosourea in mouse spermatogonia. *Proc. Natl Acad. Sci. USA* **82**, 6619–6621 (1985).

18. Shawlot, W. & Behringer, R. R. Requirement for *Lim1* in head-organizer function. *Nature* **374**, 425–430 (1995).

19. Probst, F. J. et al. Correction of deafness in *shaker-2* mice by an unconventional myosin in a BAC transgene. *Science* **280**, 1444–1447 (1998).

20. Nehls, M., Pfeifer, D., Schorpp, M., Hedrich, H. & Boehm, T. New member of the winged-helix protein family disrupted in mouse and rat *nude* mutations. *Nature* **372**, 103–107 (1994).

21. Nusslein-Volhard, C., Wieschaus, E. & Kluding, H. Mutations affecting the pattern of the larval cuticle in *Drosophila melanogaster* I. Zygotic loci on the second chromosome. *Roux Arch. Dev. Biol.* **193**, 267–282 (1984).

22. Peters, L. L. et al. Anion exchanger 1 (band 3) is required to prevent erythrocyte membrane surface loss but not to form the membrane skeleton. *Cell* **86**, 917–927 (1996).

23. Southgate, C. D., Chishti, A. H., Mitchell, B., Yi, S. J. & Palek, J. Targeted disruption of the murine erythroid band 3 gene results in spherocytosis and severe haemolytic anaemia despite a normal membrane skeleton. *Nature Genet.* **14**, 227–230 (1996).

24. Jarolim, P. et al. Mutations of conserved arginines in the membrane domain of erythroid band 3 lead to a decrease in membrane-associated band 3 and to the phenotype of hereditary spherocytosis. *Blood* **85**, 634–640 (1995).

25. Karet, F. E. et al. Mutations in the chloride-bicarbonate exchanger gene AE1 cause autosomal dominant but not autosomal recessive distal renal tubular acidosis. *Proc. Natl Acad. Sci. USA* **95**, 6337–6342 (1998).

26. Bruce, L. J. et al. Familial distal renal tubular acidosis is associated with mutations in the red cell anion exchanger (band 3, AE1) gene. *J. Clin. Invest.* **100**, 1693–1707 (1997).

27. The FANTOM Consortium and the RIKEN Genome Exploration Research Group Phase I & II Team. Analysis of the mouse transcriptome based on functional annotation of 60,770 full-length cDNAs. *Nature* **420**, 563–573 (2002).

28. Behringer, R. R. (ed.) Mouse knockout and mutation database. *BioMedNet* (<http://research.bmn.com/mkmd>) (2003).

29. Kile, B. T., Mason-Garrison, C. & Justice, M. J. Sex and strain-related differences in the peripheral blood cell values of inbred mouse strains. *Mamm. Genome* **14**, 81–85 (2003).

30. Noveroske, J. N. et al. *Quaking* is essential for blood vessel development. *Genesis* **32**, 218–230 (2002).

Supplementary Information accompanies the paper on www.nature.com/nature.

Acknowledgements We thank C. Viator, C. Dinh, S. Moncrief, A. Zalud, J. Maffucci, C. Mason-Garrison, K. Firozi, M. Alviento, C. Hubbard, B. Hasson and M. Scantlin for technical assistance, and J. Zhong and M. Patterson for database support. We also thank L. Peters for the gift of *Slc41* knockout mice. Y. Furuta, H. Bellen, S. Lovell, S. Watowich and H. Gilbert are thanked for critical reading of this manuscript. This work was supported by NIH grants to M.J.J. and A.B. K.E.H. was supported by an NIH-NRSA grant. B.T.K. is a Fellow of the Leukemia Research Foundation.

Competing interests statement The authors declare that they have no competing financial interests.

Correspondence and requests for materials should be addressed to M.J.J. (mjustice@bcm.tmc.edu).

The plastid *clpP1* protease gene is essential for plant development

Hiroshi Kuroda¹ & Pal Maliga^{1,2}

¹Waksman Institute of Microbiology, Rutgers, The State University of New Jersey, 190 Frelinghuysen Road, Piscataway, New Jersey 08854-8020, USA

²Department of Plant Biology, Rutgers, The State University of New Jersey, 59 Dudley Road, New Brunswick, New Jersey 08901, USA

Plastids of higher plants are semi-autonomous cellular organelles that have their own genome and transcription–translation machinery¹. Examples of plastid functions are photosynthesis and biosynthesis of starch, amino acids, lipids and pigments². Plastid functions are encoded in ~120 plastid genes¹ and ~3,000 nuclear genes^{2,3}. Although many embryo and seedling lethal

nuclear genes are required for chloroplast biogenesis^{4–6}, until now deletion of plastid genes either had no phenotypic consequence (8 genes), or caused a mutant phenotype but did not affect viability (13 genes)^{7–10}. Here we identify an essential plastid gene. By using the CRE–lox site-specific recombination system^{11,12} we have deleted *clpP1* (caseinolytic protease P1), one of the three genes (*clpP1*, *ycf1* and *ycf2*) whose disruption had previously only been possible in a fraction of the 1,000–10,000 plastid genome copies in a cell^{7,13}. Loss of the *clpP1* gene product, the ClpP1 protease subunit¹⁴, results in ablation of the shoot system of tobacco plants, suggesting that ClpP1-mediated protein degradation is essential for shoot development.

CRE, a site-specific recombinase derived from the P1 bacteriophage, excises any DNA sequence between two directly oriented 34-base-pair *lox* sites¹⁵. The *clpP1* exon 2 (E2) and exon 3 (E3) were first bracketed by two directly oriented *lox* sites in the plastid genome (Fig. 1a). The *clpP1* E2 and E3 encode conserved amino-acid residues essential for ClpP1 catalytic function^{14,16}. A *Cre* gene encoding a plastid-targeted CRE enzyme was then introduced into the nucleus by a sexual cross with a plant carrying a nuclear *Cre* gene. CRE, translated in the cytoplasm, was imported into all plastids and excised the *clpP1* segment between the two *lox* sites (Fig. 1b).

Tobacco plants with engineered *clpP1* genes—now flanked by *lox* sites ('floxed'), and denoted *clpP1*^{fl}—were obtained by plastid transformation. Plastid transformation was carried out with vector pHK85, in which the engineered *clpP1*^{fl} was linked with a spectinomycin resistance (*aadA*) marker gene (Fig. 2a). The transforming DNA was introduced into chloroplasts by bombardment of tobacco leaves, and transplastomic clones were selected by spectinomycin resistance. Transformed plastid genomes were obtained by replacing the plastid *clpP1* gene with the engineered *clpP1*^{fl} and *aadA* genes carried in the vector (Figs 1a and 2a). Uniform transformation of plastid genomes was confirmed by DNA gel blot analysis (lane *clpP1*^{fl}, Fig. 3a)¹⁷. Plants regenerated from the transformed tissue were indistinguishable from wild-type plants. Thus, introduction of *lox* sites and *aadA* in the *clpP1* operon did not interfere with plastid function.

Tobacco plants carrying a nuclear *Cre* gene were obtained by *Agrobacterium*-mediated transformation. The *Agrobacterium* vectors carried a *Cre* gene engineered for expression in the plant nucleus; they had a constitutive P2' promoter and a *nos* sequence encoding a polyadenylation site. The encoded CRE protein is plastid targeted because the *Cre* coding region is translationally fused at its amino terminus with a DNA segment encoding the Rubisco small subunit transit peptide (Fig. 2b).

To trigger excision of *clpP1*^{fl}, plants with engineered plastids were pollinated with nuclear *Cre* lines. Note that in tobacco only the maternal parent transmits plastids to the seed progeny, thus the seedlings carried only engineered plastids containing *clpP1*^{fl}. The *Cre* lines were maintained as heterozygotes, therefore pollination of *clpP1*^{fl} plants (maternal parent) with nuclear *Cre* lines was expected to yield seed progeny in which about half of the seedlings carried the nuclear *Cre*. It is well known that the developmental timing and level of transgene expression in the nucleus is modulated by host genome sequences adjacent to the insertion site¹⁸. Thus, we expected differences in CRE activity in the seed progeny derived from crosses with independently transformed *Cre* lines.

To evaluate the consequence of *clpP1*^{fl} excision, seed progeny derived from the crosses were germinated in sterile culture in the absence of antibiotics. Under this condition, wild-type seedlings are green (Fig. 4f). The cross of *clpP1*^{fl} plants as maternal parent and Nt-Cre30B as pollen parent¹⁹ segregated green and white progeny (302 to 317; ~1:1)(Fig. 4a). The green seedlings developed into normal plants, whereas the white seedlings failed to develop a shoot system even after ~6 months (182 days; Fig. 4b). Polymerase chain reaction (PCR) analysis confirmed that the seedlings with white